Nuclear Engineering and Technology 58 (2026) 104243

Contents lists available at ScienceDirect

Nuclear Engineering and Technology

journal homepage: www.elsevier.com/locate/net

Original Article

# Explicit and simplified modeling of in-core instrument for emitter region reaction rate calculation using STREAM/RAST-K

Kyeongwon Kim [a,1], Dongmin Yun [a,1], Wonkyeong Kim [b], Sung Ju Kwon [c], Setiawan Fathurrahman [a], Deokjung Lee [a,*]

[a] Department of Nuclear Engineering, Ulsan National Institute of Science and Technology, 50 UNIST-gil, Ulsan, 44919, Republic of Korea
[b] Core and Fuel Analysis Group, Korea Hydro & Nuclear Power Central Research Institute (KHNP-CRI), 70, Yuseong-daero 1312beon-gil, Yuseong-gu, Daejeon, 34101, Republic of Korea
[c] KEPCO NF, 242, Daedeok-daero 989 beon-gil, Yuseong-gu, Daejeon, 34057, Republic of Korea

ARTICLE INFO

*Keywords:*
In-core instrument
Self-powered neutron detector
Absorption reaction rate
STREAM/RAST-K
MCS

ABSTRACT

This study proposes an efficient and accurate method to model the In-Core Instrumentation (ICI) that utilizes Self-Powered Neutron Detectors (SPNDs) for real-time monitoring of neutron flux and power distribution in reactor cores. Traditional core analyses have often neglected the detailed ICI effects, leading to potential inaccuracies in reactivity and power predictions. The newly developed ICI models, based on simplified geometry, explicitly consider the resonance self-shielding effects on the emitter nuclide cross sections, irradiation behavior during burnup, and reactivity perturbations. The use of a two-term rational approximation significantly improves the accuracy of absorption cross sections of emitter materials compared with reference data. The reactivity effect of ICI is approximately 276 pcm for a typical Westinghouse-type fuel assembly, causing critical rod position shifts of 2–6 cm in full-core simulations. In boron-free SMR conditions, absorption reaction rates of emitters were evaluated using critical rod search calculations. Results indicate that pseudo modeling shows deviations up to 20% in end-of-cycle power predictions, whereas explicit and simplified ICI approaches consistently match with actual assembly power. Therefore, these improved ICI modeling techniques are essential for precise instrumentation and reactivity evaluation in advanced boron-free SMR cores.

## 1. Introduction

The severe environment within a nuclear reactor core makes the real-time collection of in-core operational data exceptionally difficult. Nonetheless, accurate monitoring of core power distribution is important for safe and optimized reactor operation. This monitoring is typically accomplished using In-Core Instruments (ICIs) equipped with Self-Powered Neutron Detectors (SPNDs) [1,2]. An SPND functions by measuring the electron current generated from neutron absorption in its emitter material (e.g., rhodium or cobalt) [3]. This measured signal is subsequently converted into local reactor power, providing essential data on the core's neutron flux and power profile.

The global development of enhanced-safety and high-economy Small Modular Reactors (SMRs), including South Korea's innovative-SMR, has intensified the need for improved monitoring. To boost economic efficiency, many SMRs are designed for features like load-following operation or boron-free core designs, which rely heavily on the frequent and deep insertion of control rods for reactivity control [4]. However, the localized presence and movement of control rods can induce significant power imbalances or power tilts within the core. This non-uniform power distribution can lead to localized power peaking, raising the risk of severe events such as fuel failure or departure from nucleate boiling. Therefore, accurate and high-fidelity analysis of detector signal is now more critical than ever, requiring core analysis codes capable of precisely simulating detector responses.

Currently, most core analysis codes use a pseudo ICI model. This approach treats the ICI using a homogenized material or a placeholder, failing to account for the physical complexity of the instrument [5]. This pseudo model suffers from two major deficiencies. It ignores the burnup of the SPND's emitter material over the operational cycle, and it entirely neglects the negative reactivity effect caused by the actual structural materials of the ICI. Both omissions lead to a demonstrable reduction in

* Corresponding author. Ulsan National Institute of Science and Technology, Republic of Korea.
*E-mail address:* deokjung@unist.ac.kr (D. Lee).
[1] Kyeongwon Kim and Dongmin Yun are co-first authors.

https://doi.org/10.1016/j.net.2026.104243
Received 17 November 2025; Received in revised form 28 February 2026; Accepted 2 March 2026
Available online 3 March 2026

the accuracy and reliability of the calculated core parameters and power distributions. Addressing these deficiencies is paramount for the robust safety evaluation and optimized deployment of SMRs.

To overcome these limitations, this study implements and evaluates two advanced ICI modeling techniques within the neutronics code STREAM, which are the explicit ICI model and the simplified ICI model. The explicit model represents the ICI's full geometry and material composition for the highest accuracy, while the simplified model offers a more practical, less computationally demanding alternative suitable for general implementation in various lattice codes.

The structure of the paper is as follows. Section 2 explains the conventional pseudo ICI modeling, the proposed explicit ICI modeling, and the simplified ICI modeling techniques. Section 3 compares and analyzes the reactivity effect when the explicit ICI modeling and the simplified ICI modeling are applied to a 2D fuel assembly. Section 4 compares the absorption reaction rate in the emitter region during burnup calculations using both the explicit and simplified ICI models. Finally, Section 5 presents the results of the whole-core reaction rate calculation and signal-to-power consistency calculation using the STREAM/RAST-K. The lattice physics code STREAM, the nodal diffusion code RAST-K v2, and the Monte Carlo neutron and photon transport code MCS are utilized in this study [6–8]. All three codes have been developed by the COmputational Reactor physics and Experiment (CORE) laboratory at the Ulsan National Institute of Science and Technology (UNIST).

The results of this work will clearly demonstrate the quantitative impact of explicitly considering the ICI, a factor often neglected in conventional analyses, and will propose both the high-fidelity explicit modeling approach and the computationally advantageous simplified modeling approach for future reactor simulations.

## 2. ICI modeling

The SPND signal, represented to the neutron absorption reaction rate of emitter nuclides in RAST-K, is defined as Eq. (1).

$$RR(r,z) = N^{det}\sum_{g}\sigma_{g}^{det}\phi_{g}^{det}(r,z) \quad \text{Eq. (1)}$$

Where $N^{det}$ and $\sigma_g^{det}$ are the number density and absorption cross-section (XS) of emitter nuclides, and $\phi_g^{det}(r,z) = \alpha_g^{det}\phi_g$ is the local flux at the emitter region, which is multiplied by pin-to-box factor ($\alpha_g^{det}$) for SPND from the nodal flux ($\phi_g$). Those detector parameters are calculated from STREAM during the generation of group constants with respect to the case matrix.

Most lattice codes, including STREAM, can only model symmetric structures where the center of the circle is at the center of the lattice. However, as Fig. 1 shows the Rh ICI and V ICI, SPND within the ICI is difficult to model with lattice codes because its circular center is not at the lattice center [9]. To address this complexity and generate $\sigma_g^{det}$, the pseudo, simplified, and explicit methods are used for geometry, resonance treatment, and the neutron irradiation effects of emitter nuclides.

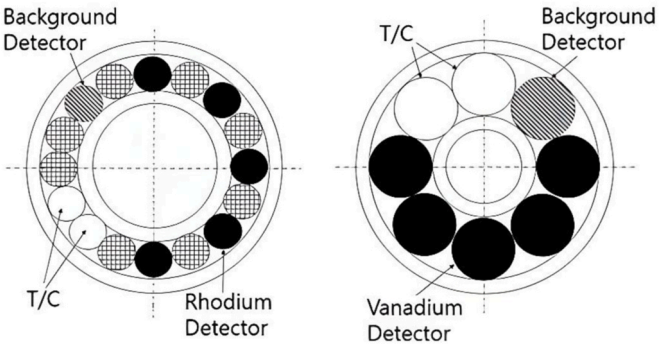


**Fig. 1.** Cross-sectional view of Rh ICI (left) and V ICI (right).

### 2.1. Pseudo ICI modeling

For the pseudo ICI model, which is widely used for practical core design method of lattice code, the absorption XS of the emitter region is calculated using a virtual pseudo flux at the center of an empty instrument tube filled only with moderator. This approach assumes that the actual insertion of ICI at the center of the instrument tube has negligible effect on neutronic behavior, particularly the criticality of the fuel assembly. Based on geometry-dependent constant background XS and corresponding resonance integral table, the resonance treatment of the emitter nuclide's multi-group XS is performed using the equivalence theory, a widely applied resonance self-shielding method [10]. For a typical cylindrical Rh emitter with a radius of 0.23 mm, the $n$-th background XS term of nuclide $r$, $\sigma_{b,n,g}^{r} = 582$ barns, is used to interpolate the pre-calculated resonance integral form for determining the effective XS.

### 2.2. Explicit ICI modeling

A new indexing scheme was developed for STREAM to allow for the representation of ICI structures with explicit geometry in two-dimensional assembly problems, supplementing the conventional concentric cell-type indexing system. By mapping the flat source region (FSR) indices within the guide tube structure, as illustrated in Fig. 2, the corresponding indices for material properties and multi-group XS data are then assigned.

Given the actual FSR indices and material compositions, the local neutron flux and escape probability within the emitter region can be evaluated explicitly. Since rhodium and cobalt are the dominant nuclides in the emitter material and exhibit pronounced resonance behavior, a more rigorous resonance self-shielding treatment is required. Accordingly, the inner SPND geometry, including the emitter, insulator, and collector, is modeled as a heterogeneous isolated system, enabling an explicit treatment of resonance effects within each constituent region.

When applying equivalence theory to SPND in a heterogeneous isolated system, the neutron spectrum assumption is reformulated to reflect

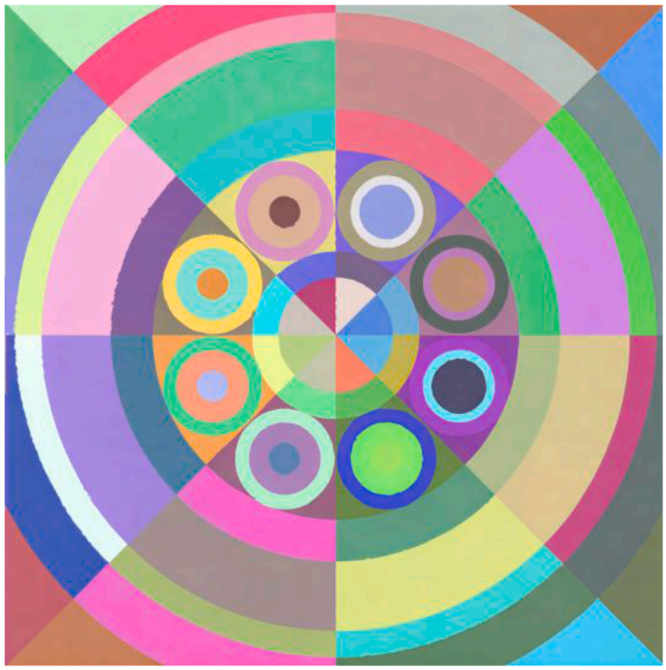

**Fig. 2.** FSR plot for explicit geometry of ICI by STREAM.

SPND-specific physics rather than fuel resonance absorption. The focus is placed on local neutron interactions governing electron emission, gamma production, and short-range particle transport. Here, the escape probability is redefined specifically for the detector emitter region. It is defined as the probability that a neutron entering the emitter region escapes from the emitter without undergoing any collision within the emitter material. Neutron behavior within the emitter is described using a first-flight assumption. Neutrons are assumed to travel freely within the emitter until their first interaction, and the absorption probability in the emitter is expressed in terms of an escape-probability formulation using the average chord length $\bar{l}$ and the energy-dependent total macroscopic cross section $\Sigma_t^e(E)$. Neutron leakage from the emitter into surrounding regions (insulator and collector) is treated analogously to fuel–moderator problems by introducing an equivalent background cross section, $\Sigma_{e,eq}$, which incorporates geometric effects and the influence of the surrounding materials.

The energy-dependent escape probability, $P_e(E)$, is evaluated using two-term rational approximations tailored to the geometry of each resonant region. For cylindrical geometries, which apply to the emitter material, Carlvik's two-term rational approximation is employed. For slab-like geometries, which are used to represent the insulator, collector, and sheath regions modeled as ring-type resonant structures, Roman's two-term rational approximation is adopted. These formulations are expressed as Eq. (2), and Eq. (3).

$$P_{e,Calvik}(E) = 2\frac{2}{\Sigma_t(E)\bar{l}+2} - \frac{3}{\Sigma_t(E)\bar{l}+3} \quad \text{Eq. (2)}$$

$$P_{e,Roman}(E) = 1.1\frac{1.4}{\Sigma_t(E)\bar{l}+1.4} - 0.1\frac{5.4}{\Sigma_t(E)\bar{l}+5.4} \quad \text{Eq. (3)}$$

For cylindrical geometry, which is applied to the emitter material, Carlvik's constants are determined by satisfying the white and black limits of average emitter-to-emitter first-flight collision probability $\widetilde{P}_{FF}$ and its first derivative. Otherwise, for slab geometry, which is applied to the insulator, collector, and sheath structures as ring-type resonant materials, Roman identified a suitable choice of constants to minimize the error of $P_e$ in the two-term rational approximation. Therefore, the resonance self-shielding treatment of the insulator and collector materials is performed using Roman's two-term rational approximation and Carlvik's two-term rational approximation for the cylindrical emitter region [11].

Within the newly defined SPND lattice geometry, it is further assumed that the emitter nuclide in each FSR is unique. As a result, inter-emitter shadowing effects on neutron escape are negligible, implying that the Dancoff factor is approximately zero. The list of resonant nuclides are from basic decay chain of rhodium-103 and cobalt-60.

Table 1 present the two-group effective absorption XSs of emitter nuclides obtained with the pseudo and explicit geometry models in a fuel assembly. It is confirmed that absorption XS of Carlvik/Roman N-term rational approximation within the equivalence theory.

The explicit ICI modeling scheme requires significantly higher computational cost. In order to accurately resolve the detailed geometry, the ray spacing for the MOC (Method of Characteristics) calculation must be considerably smaller than the radius of the smallest emitter, which is less than 0.1 mm for a Rh emitter with a radius of 0.3 mm. Moreover, because the explicit ICI geometry consists of eight asymmetrically arranged thimbles, the octant symmetry feature commonly used in lattice analysis cannot be applied, further increasing the computational burden.

**Table 1**
Rh-103 and Co-59 absorption XS with respect to geometry scheme.

| ICI Modeling | Rh-103 | | Co-59 | |
|---|---|---|---|---|
| | $\sigma_{a,1}$ | $\sigma_{a,2}$ | $\sigma_{a,1}$ | $\sigma_{a,2}$ |
| MCS(Explicit) | 11.14 | 88.37 | 1.19 | 19.45 |
| STREAM(Pseudo) | 30.68 | 92.33 | 2.94 | 20.90 |
| STREAM(Explicit) | 11.10 | 88.40 | 1.14 | 19.45 |

### 2.3. Simplified ICI modeling

Generally, a fuel assembly has an 1/8 symmetry, so simulations are usually performed on an 1/8 section of the fuel assembly. However, because the ICI lacks this symmetry, a full fuel assembly must be simulated, which increases computation time by a factor of approximately eight. To address this issue, a simplified ICI model was developed and is shown in Fig. 3. The left side of Fig. 3 shows a Co-centered simplified ICI model (Co-simplified ICI model) with the Co emitter at the center, while the right side shows a Rh-centered simplified ICI model (Rh-simplified ICI model) with the Rh emitter at the center.

The simplified ICI model is constructed by placing either a Co-SPND or a Rh-SPND at the center of the lattice. The material regions of the ICI components, such as the tubes, thimbles, and void spaces, are rearranged while maintaining their original volume. Since two types of SPNDs, Co-SPND and Rh-SPND, are used in the ICI, there are two distinct simplified ICI models, each with one of the SPND types positioned at the center.

The resonance treatments of emitter nuclide at simplified ICI model are implemented solving fixed source problem on the accounted local flux. For each model on Fig. 3, the escape probabilities from Calvik's two-term rational approximation are adjusted on resonant nuclides of centered emitter. Table 2 shows the emitter material resonance treatment method for each ICI model.

A comparative analysis was performed in the next section to determine if the simplified ICI model preserves the reactivity and the absorption reaction rate in the emitter region of the explicit ICI model.

## 3. Reactivity analysis

The fuel assembly used for reactivity analysis is a Westinghouse-type with a 17-by-17 array of fuel pin-cells. It consists of 243 fuel rods, 16 burnable absorber rods, 29 guide tubes, and 1 instrument tube. The ICI is located in the instrument tube. Fig. 4 shows the 2D fuel assembly used for reactivity analysis.

### 3.1. Analysis of the effect of ICI on the reactivity

When an ICI is inserted into the instrument tube of a fuel assembly, it causes a reduction in reactivity. This analysis focused on identifying the specific materials within the ICI that contribute to this reactivity decrease and quantifying their effect. The analysis was performed using MCS. The MCS was chosen for its high degree of modeling flexibility, which is essential for accurately simulating the complex geometry and material composition of the fuel assembly and the inserted ICI. Table 3 shows the effect of each material constituting the ICI by calculating the $k_{inf}$ after replacing specific materials with a void. The standard deviation of $k_{inf}$ calculated using MCS is 3-4 pcm.

Based on the results shown in Table 3, the insertion of an ICI into the 2D fuel assembly reduces reactivity by 276 pcm. By replacing each of the materials used in the ICI with a void, the effect of each material was analyzed. The reactivity decrease due to the exclusion of the moderator in the ICI region is 41 pcm. When the Inconel material of the ICI tubes and thimbles is replaced with a void, reactivity decreases by 118 pcm. This means that Inconel is responsible for a reactivity reduction of 158 pcm (276-118). The reactivity reduction caused by the Co and Rh emitter materials is 26 pcm (276-250) and 28 pcm (276-248), respectively. To evaluate the effect of ICI insertion on reactivity during burnup, calculation was performed using the STREAM, in which the burnup effect of both Rh and Co were explicitly considered. Fig. 5 shows the difference in $k_{inf}$ over burnup calculations for a 2D fuel assembly without an ICI and one with ICI.

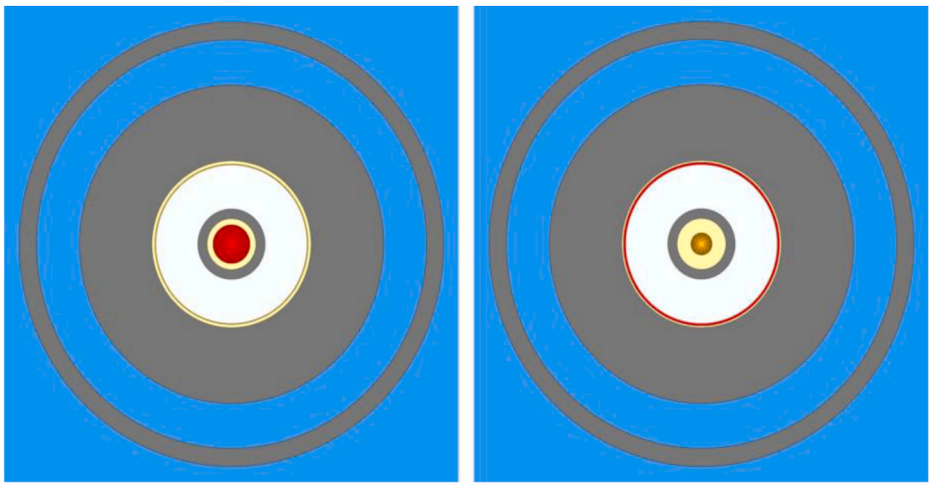

**Fig. 3.** Co-centered simplified ICI model (left) and Rh-centered simplified ICI model (right).

**Table 2**
Resonance treatment methods in emitter region.

| ICI Modeling | Resonance treatment method | |
|---|---|---|
| | Rh | Co |
| Pseudo ICI | Equivalence theory | Equivalence theory |
| Co-centered simplified ICI | Roman's approximation | Calvik's approximation |
| Rh-centered simplified ICI | Calvik's approximation | Roman's approximation |
| Explicit ICI | Calvik's approximation | Calvik's approximation |

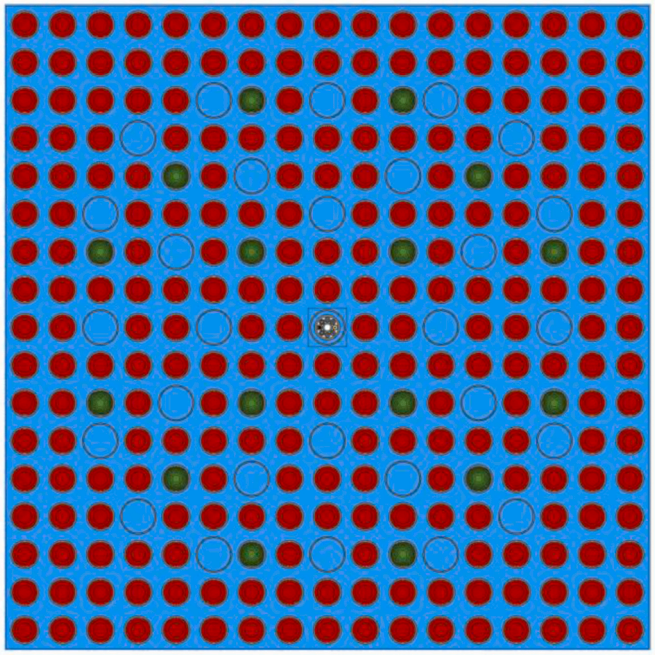

**Fig. 4.** Configuration of Westinghouse-type fuel assembly.

As shown in Fig. 5, when the ICI is inserted into the 2D fuel assembly, the reactivity decreases by approximately 200–300 pcm up to a burnup of 30 MWd/kgU, and by approximately 100 pcm at a burnup of 60 MWd/kgU.

### 3.2. Comparison of explicit ICI model and simplified ICI model

Burnup calculations were performed to compare the differences in $k_{inf}$ over burnup for a 2D fuel assembly with an explicit ICI model, a Co-simplified ICI model, and a Rh-simplified ICI model, respectively. Fig. 6 compares the results for a 2D fuel assembly with an explicit ICI model to a 2D fuel assembly with a Co-simplified ICI model, and also compares the results for an explicit ICI model to a Rh-simplified ICI model.

The maximum $k_{inf}$ difference in the 2D fuel assembly is 42 pcm between the Co-simplified ICI and explicit ICI models, and 30 pcm between the Rh-simplified ICI and explicit ICI models, as depicted in Fig. 6. Furthermore, the maximum difference in $k_{inf}$ between the Co-simplified ICI model and the Rh-simplified ICI model occurs at a burnup of 0 MWd/kgU, with a value of 21 pcm.

**Table 3**
Effect of each material constituting the ICI.

| Case | $k_{inf}$ | Diff. [pcm] |
|---|---|---|
| Reference: 2D fuel assembly | 1.15158 | reference |
| Base Case: ICI inserted | 1.14882 | −276 |
| Void in ICI region | 1.15117 | −41 |
| Void in Co emitter material | 1.14908 | −250 |
| Void in Rh emitter material | 1.14910 | −248 |
| Void in Inconel material | 1.15040 | −118 |
| Void in insulator region | 1.14886 | −272 |
| Void in collector region | 1.14890 | −268 |

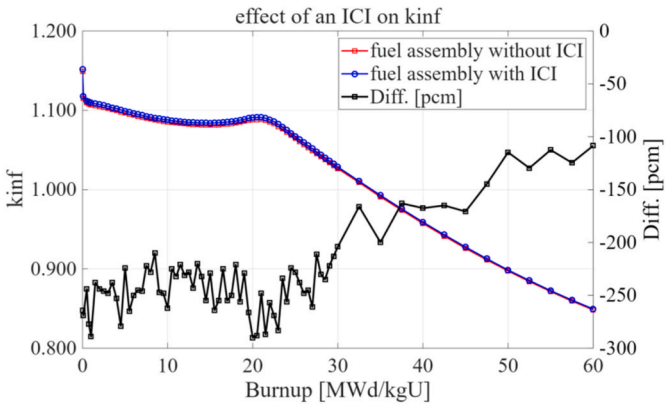


**Fig. 5.** Effect of an ICI on kinf over burnup of a 2D fuel assembly.

## 4. Analysis of absorption reaction rate in emitter region

The 2D fuel assembly used for reactivity analysis was also utilized for

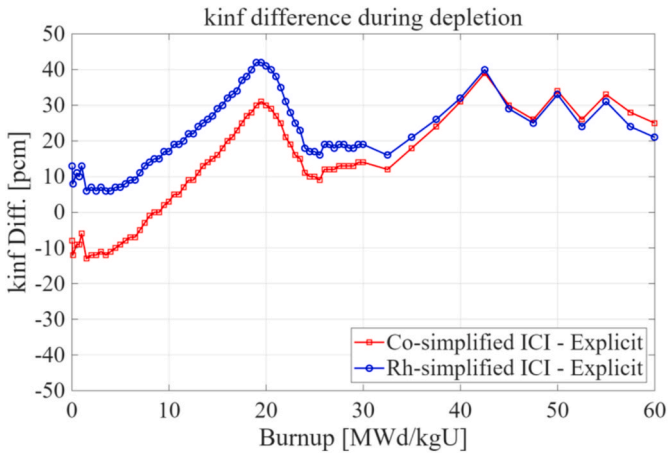


**Fig. 6.** The difference in kinf according to the insertion of explicit ICI and simplified ICI.

the analysis of the absorption reaction rate in the emitter region. Calculations were performed to determine the burnup-dependent absorption reaction rates for the Co and Rh emitter regions in a 2D fuel assembly with an explicit ICI model using MCS, and these results were established as the reference. STREAM was used to produce calculation results for the burnup-dependent absorption reaction rates in the Co and Rh emitter regions of a 2D fuel assembly with a Co-simplified ICI model and a Rh-simplified ICI model. The relative standard deviations of the absorption reaction rates for the Co and Rh emitter regions calculated by MCS are 0.48% and 0.78%, respectively. Figs. 7 and 8 show the comparison results of the absorption reaction rates for the Co emitter region and the Rh emitter region, respectively. Here, the absorption reaction rate of the emitter region includes those of all isotopes generated through the burnup of Co and Rh.

As shown in Fig. 7, the absorption reaction rate for the Co emitter region calculated by STREAM with the Co-simplified ICI model is closer to the result calculated by MCS with the explicit ICI model than to the result calculated by STREAM with the explicit ICI. The average difference between the results from STREAM (Co-simplified ICI) and MCS (explicit ICI) is 0.77%, while the average difference between the results from STREAM (Co-simplified ICI) and STREAM (explicit ICI) is 3.96%. Conversely, as shown in Fig. 8, the absorption reaction rate for the Rh emitter region calculated by STREAM with the explicit ICI model is closer to the result calculated by MCS with the explicit ICI model than to the result calculated by STREAM with the Rh-simplified ICI. The average difference between the results from STREAM (Rh-simplified ICI) and MCS (explicit ICI) is 2.04%, while the average difference between the results from STREAM (Rh-simplified ICI) and STREAM (explicit ICI) is 1.05%.

The absorption reaction rate is expressed in Eq. (1) as the product of the number of neutrons, number density, and absorption microscopic XS. In this calculation, the number density and absorption microscopic XS account for all nuclides generated through the burnup and decay of the Co and Rh emitters. Fig. 9 presents the variations in the number of neutrons, number density, and absorption microscopic XS according to the burnup of both emitters. Each value has been normalized to an average of 1.0 to facilitate a comparative analysis of their functional shapes. For the Co emitter, as burnup progresses, the number density within the emitter region tends to decrease, while the absorption microscopic XS shows a slight increase. Due to the significant variation in the number of neutrons, the absorption reaction rate of the Co emitter region exhibits a trend similar to the shape of the neutron population. In contrast, for the Rh emitter, the number density within the emitter region remains relatively constant during burnup. However, the absorption microscopic XS decreases while the number of neutrons increases as burnup proceeds. These results are generated using the STREAM with a simplified ICI model.

## 5. Comparison of absorption reaction rate in emitter region and power

### 5.1. Whole-core ICI modeling

An boron-free SMR core was analyzed by inserting a pseudo ICI model, an explicit ICI model, and a simplified ICI model into a specific fuel assembly, respectively. Fig. 10 shows the SMR core loading pattern and the locations of the fuel assemblies equipped with ICI. In this study, it was assumed that the emitter is fully inserted axially to produce and compare precise calculation results. STREAM performs calculations for both instrumented and uninstrumented fuel assemblies through predefined case matrix branches, while RAST-K arranges and stacks the corresponding group constant data according to the SMR loading pattern specified in the design data.

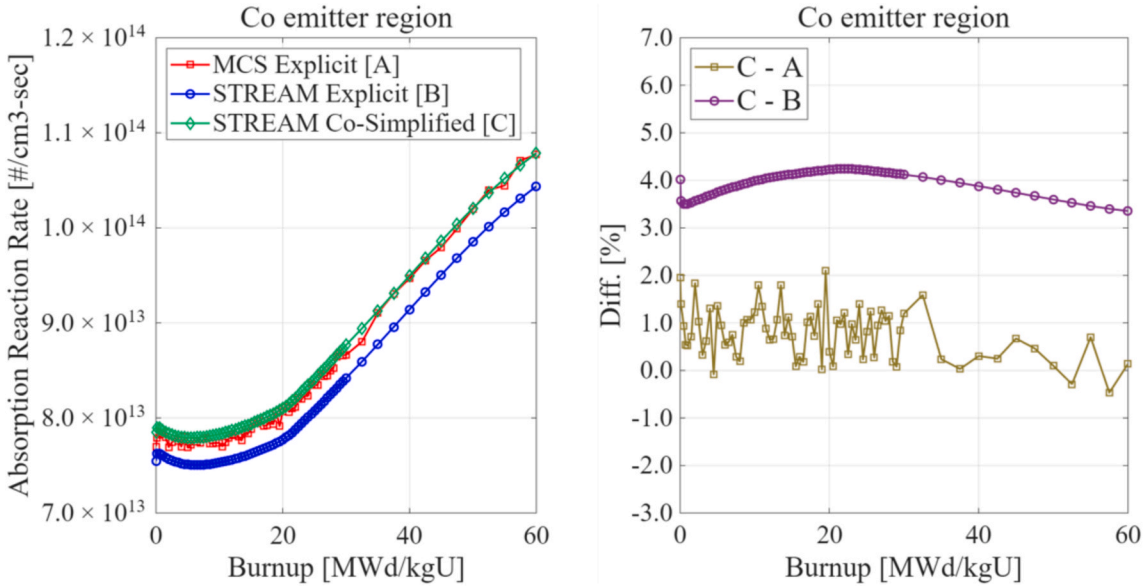


**Fig. 7.** Comparison of absorption reaction rate for the Co emitter region.

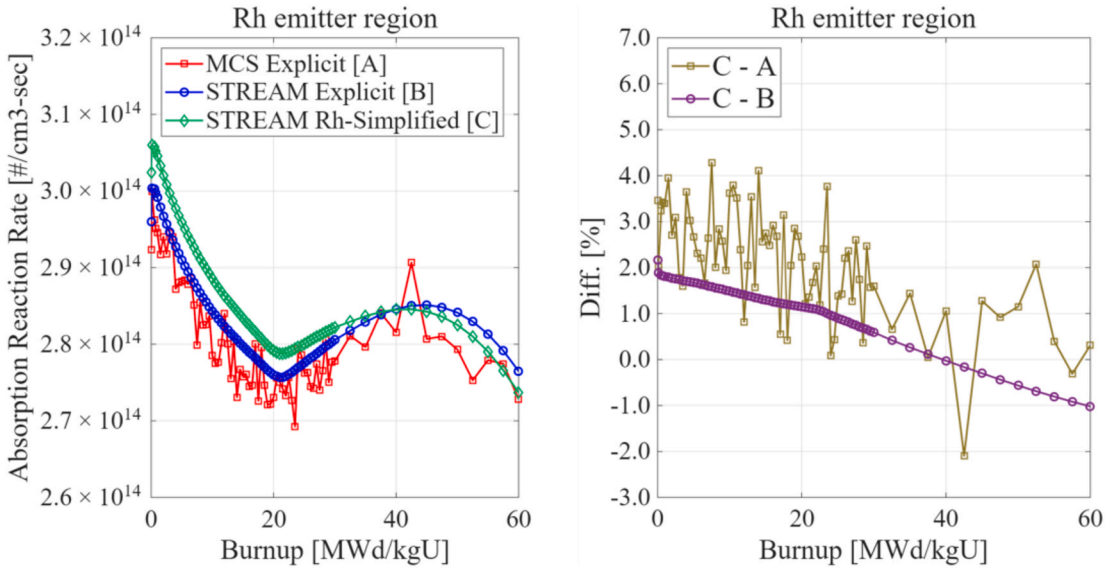


**Fig. 8.** Comparison of absorption reaction rate for the Rh emitter region.

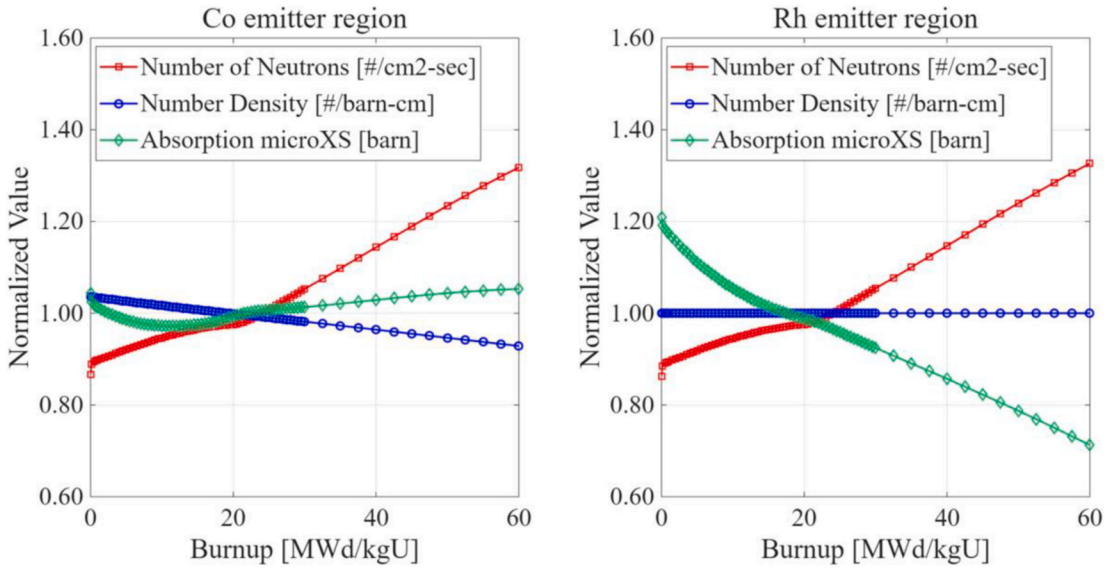


**Fig. 9.** Comparison of absorption reaction rate for the Rh emitter region.

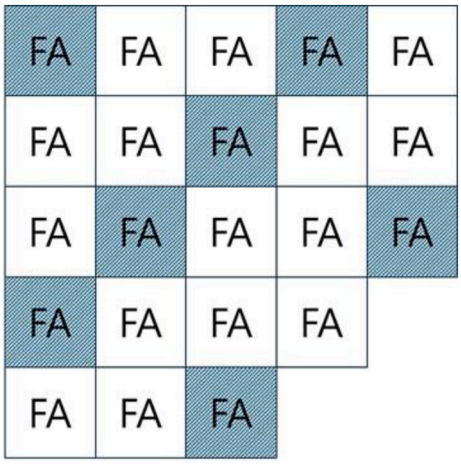


**Fig. 10.** SMR core loading pattern (fuel assemblies with ICI are shaded).

### 5.2. *Effect of ICI on the whole-core depletion*

In the whole-core loading pattern design, the effects of ICIs observed in the two-dimensional assembly analysis are mitigated due to their radially and axially sparse installation. To quantify the effect of ICIs on reactivity, a hot full power, all-rods-out (HFP ARO) depletion calculation was performed, as shown in Fig. 11. The pseudo ICI modeling uses a fuel assembly without ICIs, whereas the explicit and simplified ICI modeling approaches use assemblies with ICIs inserted. The whole-core effective multiplication factor ($k_{eff}$) obtained using ICI-inserted assemblies is approximately 50 to 60 pcm lower than that of the core modeled without ICIs. The reactivity difference between the explicit and simplified ICI models is approximately 3 to 5 pcm.

For a more realistic simulation, the whole-core depletion calculation was performed in the critical rod search mode of RAST-K. The positions of the leading regulating control banks were adjusted to compensate for excess positive reactivity, following the prescribed overlap rule. The resulting critical rod positions are shown in Fig. 12, exhibiting an inverse trend relative to the ARO $k_{eff}$ results in Fig. 11. The presence of ICIs

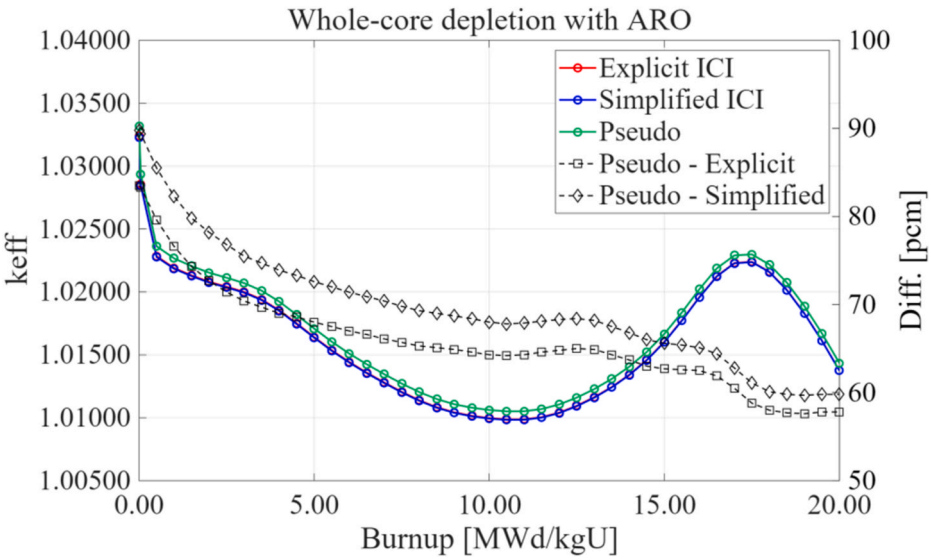


**Fig. 11.** HFP ARO depletion of boron-free SMR with respect to ICI modeling methods.

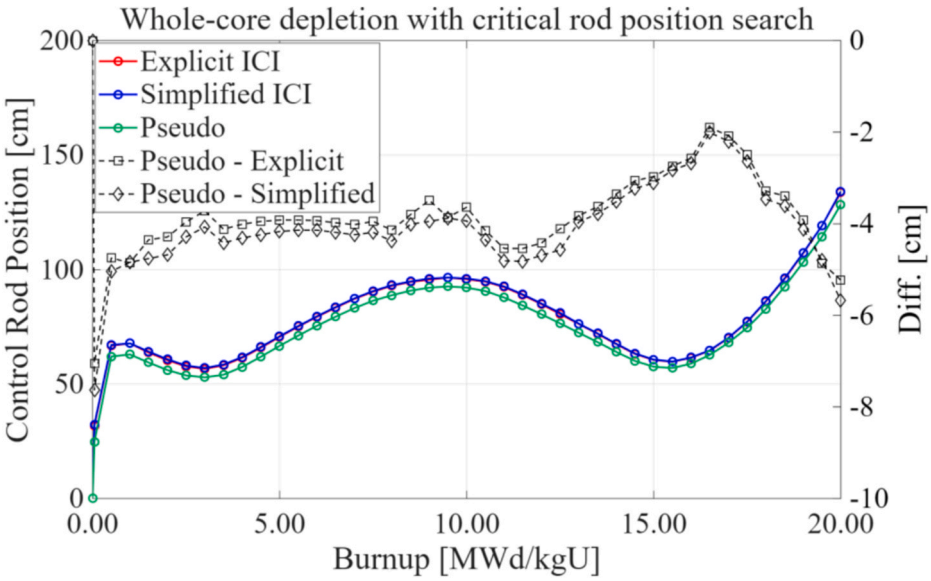


**Fig. 12.** Critical rod search depletion of boron-free SMR with respect to ICI modeling methods.

causes the critical rod positions to shift by approximately 2 to 6 cm, while the difference between the explicit and simplified ICI models is about 0.1 to 0.5 cm.

### 5.3. Two-group condensation for whole-core reaction rate calculation

Using the detailed analysis data obtained from the newly developed ICI modeling scheme, RAST-K generates group constants for whole-core detector signal analysis according to Eq. (1). The fast and thermal group constants, $\sigma_g^{det}$ and $\alpha_g^{det}\left(=\phi_g^{det}/\phi_g^{FA}\right)$ are derived through the required case matrices in RAST-K. The group constants for the reference cases are presented in Fig. 13, which is extended through burnup from the data summarized in Table 1. During the group condensation process, the local flux differences at the actual detector positions and the effects of explicit resonance treatment influence all types of group constants. Most burnup-dependent group constants exhibit noticeable changes around the inflection point corresponding to the depletion of gadolinia.

### 5.4. Irradiation effect of emitter nuclides

During the power operation, the emitter nuclides in SPND are continuously exposed by neutron irradiation. Since the main principle of the SPND is to measure electrons, the emitter nuclei are inevitably activated by neutrons, leading to a reduction in their number and the production of secondary products. In RAST-K, an independent target irradiation (ITI) module for a given target sample has been developed to enable these processes to be simulated within a whole-core depletion environment.

The ITI module solves the independent Bateman equation of decay chain of initial emitter's nuclide, i.e. cobalt-59, and rhodium-103. In RAST-K, the time evolution of $N^{det}$ over a time step was solved using the Chebyshev Rational Approximation Method (CRAM) [7]. This module requires local fluxes at the specific target emitter that can be obtain using the nodal flux ($\phi_g^{FA}$) and emitter-to-box factor $\alpha_g^{det}$. When employing on-the-fly fluxes for ITI calculations, the results exhibit a strong dependence on the axial power shape and flux integration,

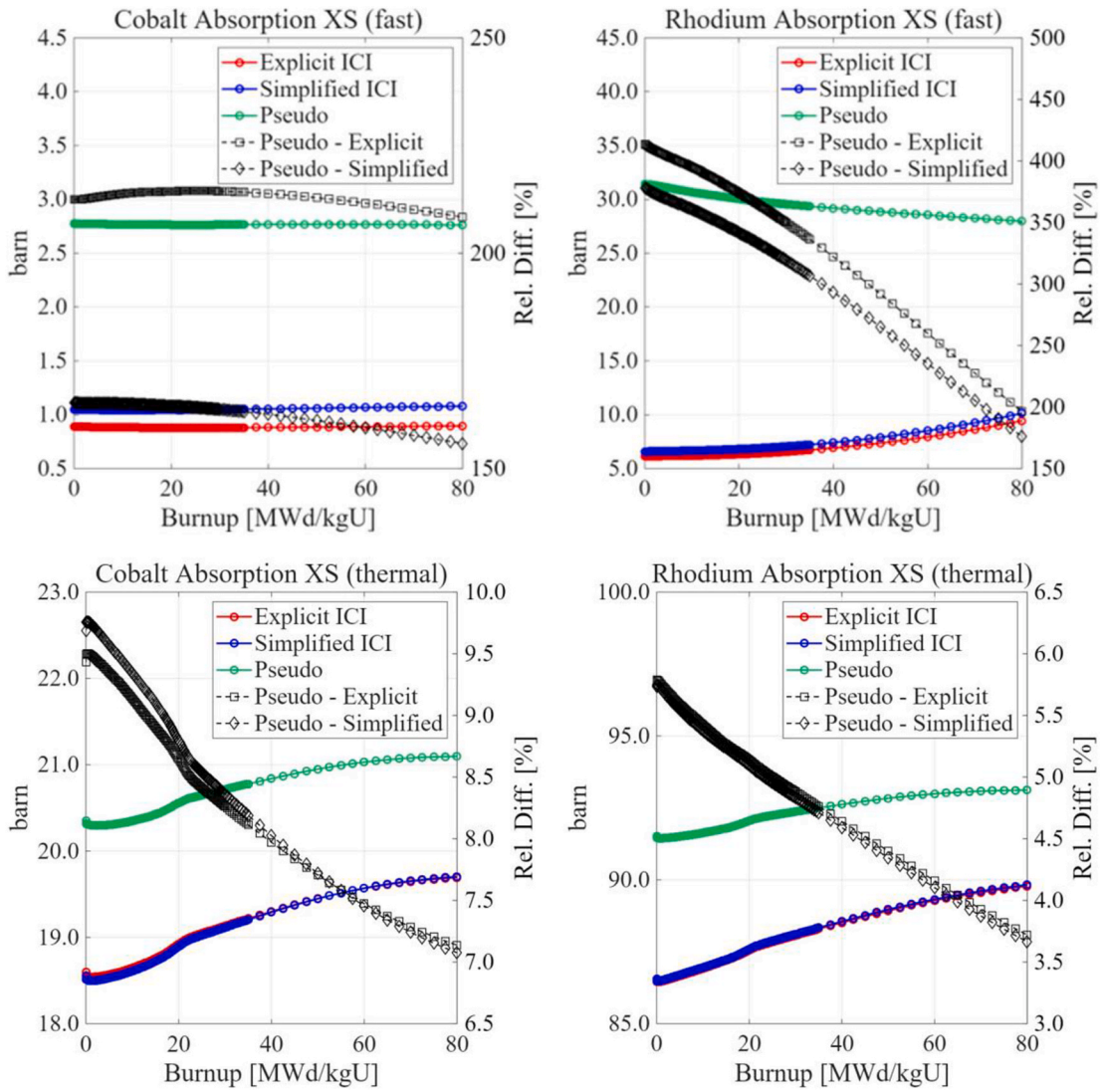


**Fig. 13.** Group-wise neutron absorption XS ($\sigma_g^{det}$) of Co and Rh emitter.

particularly in terms of the emitter-to-box factor values.

As shown in Fig. 13, the absorption cross section of rhodium-103 is significantly higher than that of cobalt-59. Furthermore, Fig. 14 indicates that the thermal emitter-to-box factors obtained using the pseudo method are overestimated due to the presence of a "pseudo moderator" instead of the actual ICI structure.

Based on these irradiation effects, the number density of each emitter ($N^{det}$ of Eq (1)) has been estimated throughout the whole-core depletion calculation. The relative number density at end of cycle (EOC), expressed as $N_t^{det}/N_0^{det}$ is shown in Fig. 15. The results reveal that the effect is more pronounced for rhodium-103 and that the explicit method provides a more accurate representation. There are axially heterogeneous irradiation effects due to axial power profile.

### 5.5. Comparison of absorption reaction rate in emitter region and power

The data required for the reaction rate calculation in Eq. (1) within the two-group nodal code RAST-K were obtained from the group constant generation process of STREAM. In this section, the SPND reaction rates are compared across different XS modeling schemes—pseudo, simplified, and explicit. In the simplified and explicit methods, the effects of local neutron flux and actual irradiation effect are directly incorporated into the XS data, whereas the pseudo method neglects these effects. Nevertheless, in the whole-core simulation, SPND irradiation effect is still considered using the local flux computed by RAST-K.

Fig. 16 illustrates the radial distribution of reaction rates within the instrumented assembly at EOC and EOC using fresh emitter ($N_t^{det}/N_0^{det} = 1$). The right side of Fig. 16 represents the relative difference (RD) between the normalized assembly power and reaction rates for each assembly. At EOC, the root mean square(RMS) of RDof rhodium reaction rates calculated using the pseudo method is 11.58%. This RD is even higher than those of explicit and simple method, respectively 0.73%, and 1.07%. On the other hand, in cases of cobalt emitter using pseudo method which is less affected by irradiation, the RMS of RD is resulted with 2.36%. The following results demonstrate that the pseudo method can lead to inaccuracies when designing new types of ICIs.

Figs. 17 and 18 show the normalized assembly power and the corresponding normalized reaction rates of cobalt and rhodium emitters as functions of burnup. For the rhodium emitter in the pseudo modeling case, the reaction rate calculated with the burned number density changes significantly with increasing burnup. Conventional pseudo modeling assumes a fresh emitter number density with empirical burnup compensation; however, for new instrumentation systems such as those used in SMRs, where no predefined compensation exists, the use of the actual burned emitter composition is essential. As shown in Fig. 17, only the explicit and simplified modeling approaches can accurately capture

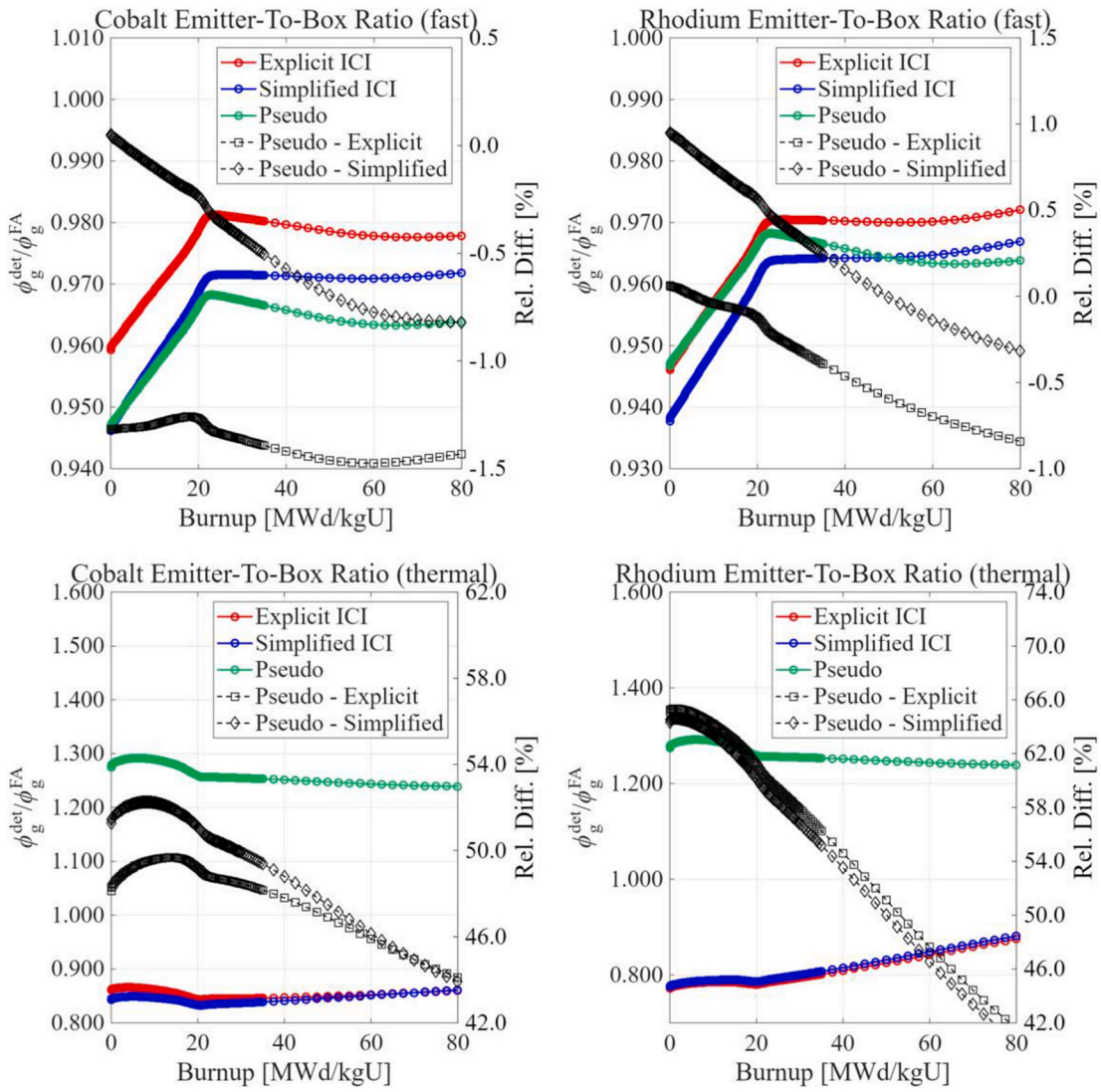


**Fig. 14.** Group-wise emitter-to-box ratio ($\alpha_g^{det}$) of Co and Rh emitter.

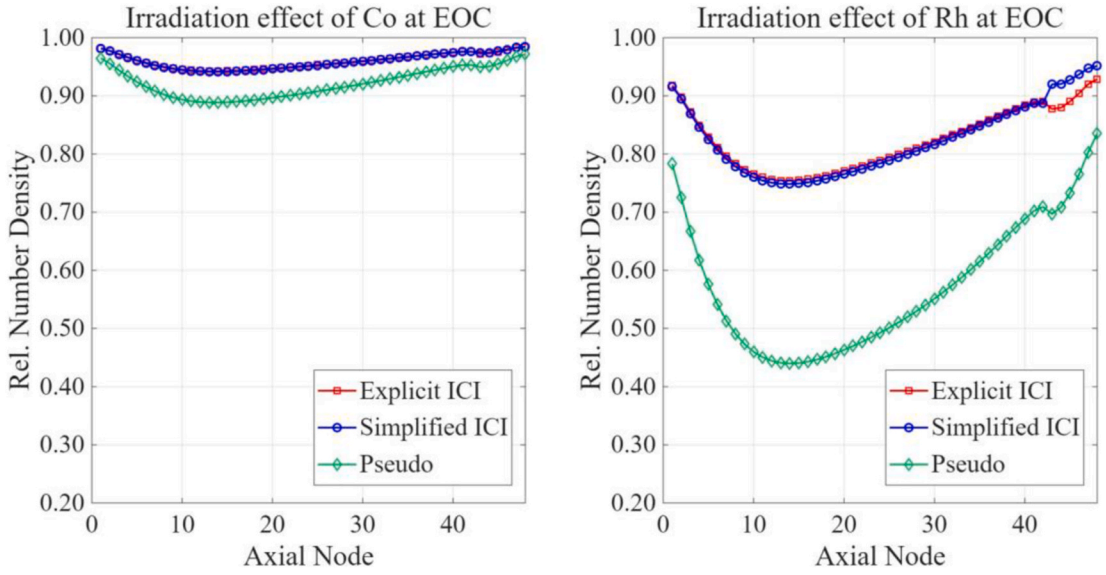


**Fig. 15.** Neutron irradiation effects on emitter nuclides at EOC, Center FA.

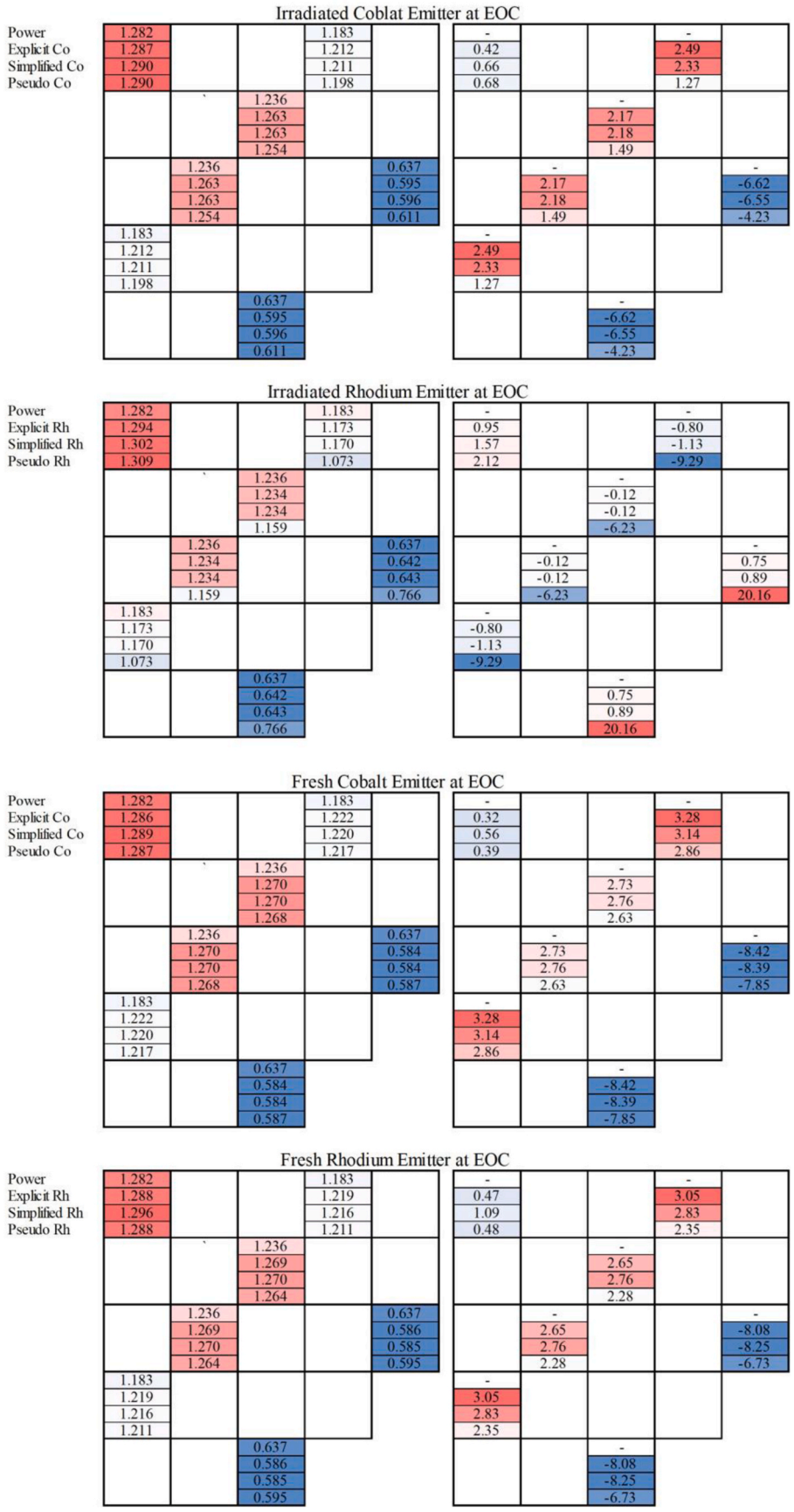


**Fig. 16.** Radial power and reaction rates, and those relative differences.

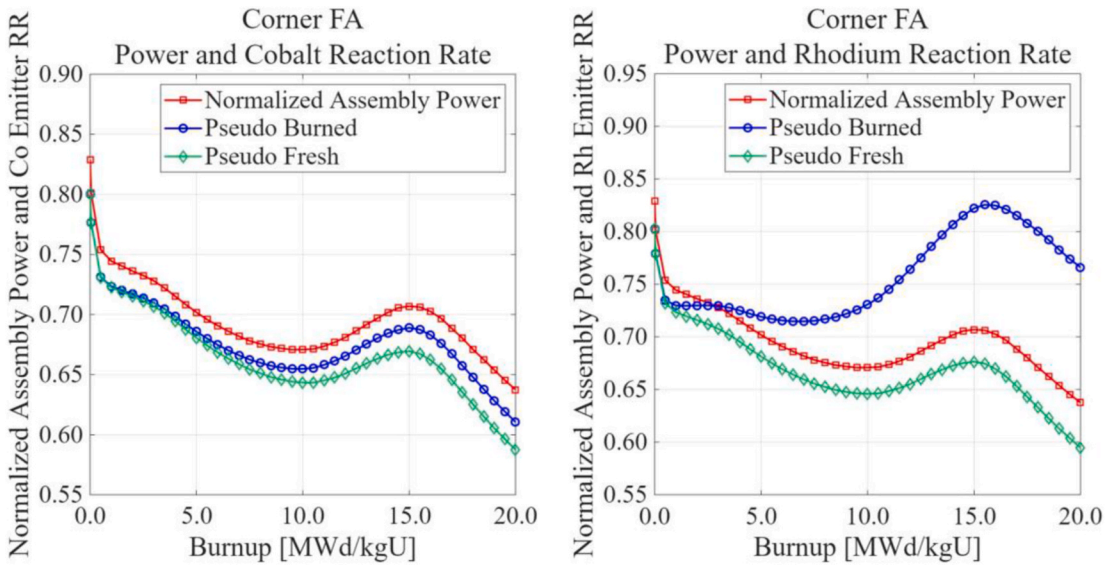


**Fig. 17.** Normalized assembly power and corresponding reaction rate of cobalt and rhodium emitter of pseudo model, in terms of burnup dependency of emitter in RAST-K.

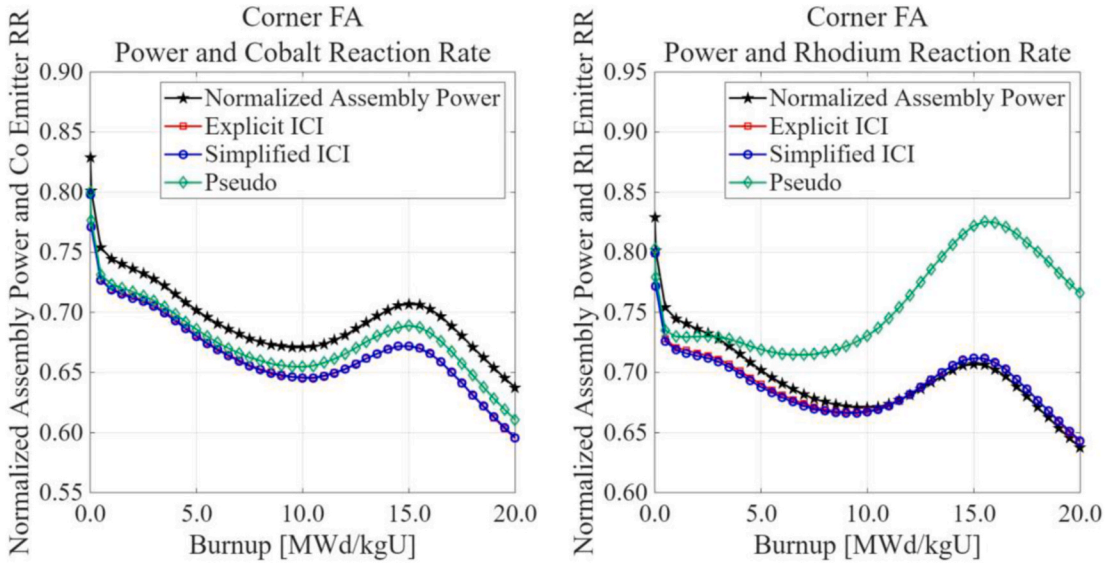


**Fig. 18.** Normalized assembly power and corresponding relative differences from reaction rate of cobalt and rhodium emitter, in terms of modeling methods.

the strong burnup-dependent behavior of the rhodium emitter and reproduce the assembly power distribution.

Figs. 19 and 20 present the axial power distributions and the corresponding axial reaction rates at the end of the cycle. Similar to the radial results in Fig. 16, the pseudo modeling approach for the rhodium emitter fails to follow the actual axial power shape. This deviation arises because the pseudo model relies on an overestimated moderator flux and neglects resonance self-shielding effects, leading to exaggerated irradiation predictions. Moreover, although RAST-K updates the emitter number density $N_t^{det}$, as a burnup-dependent variable, the pseudo XS data from STREAM remain static and do not reflect spectral or self-shielding variations with burnup. This inconsistency between the evolving isotopic composition and the fixed XS data causes a noticeable signal-to-power mismatch, as seen in Fig. 20. In contrast, the explicit and simplified modeling schemes capture the actual ICI insertion geometry and properly account for resonance self-shielding effects. Consequently, the XS data remain consistent with the burnup-dependent reaction rates, enabling the calculated SPND reaction rates to accurately follow both the radial and axial assembly power distributions.

## 6. Conclusion

This study successfully developed and validated new ICI modeling using STREAM/RAST-K to address the critical inaccuracies associated with traditional core analysis that relies on an inadequate pseudo method. Both an explicit ICI model and a simplified ICI model were introduced, designed to accurately account for the structural and neutronic effects of the ICI while minimizing computational cost. The simplified model, in particular, proved highly effective by preserving the 1/8 fuel assembly symmetry. This allowed it to maintain computational efficiency comparable to conventional analyses, with a maximum $k_{inf}$ difference of only 42 pcm from the explicit model in the fuel assembly.

The results of this study confirmed the physical necessity of accurate ICI modeling. The insertion of the ICI was shown to induce a significant negative reactivity effect of approximately 276 pcm. Consequently, whole-core simulations of a boron-free SMR demonstrated a noticeable

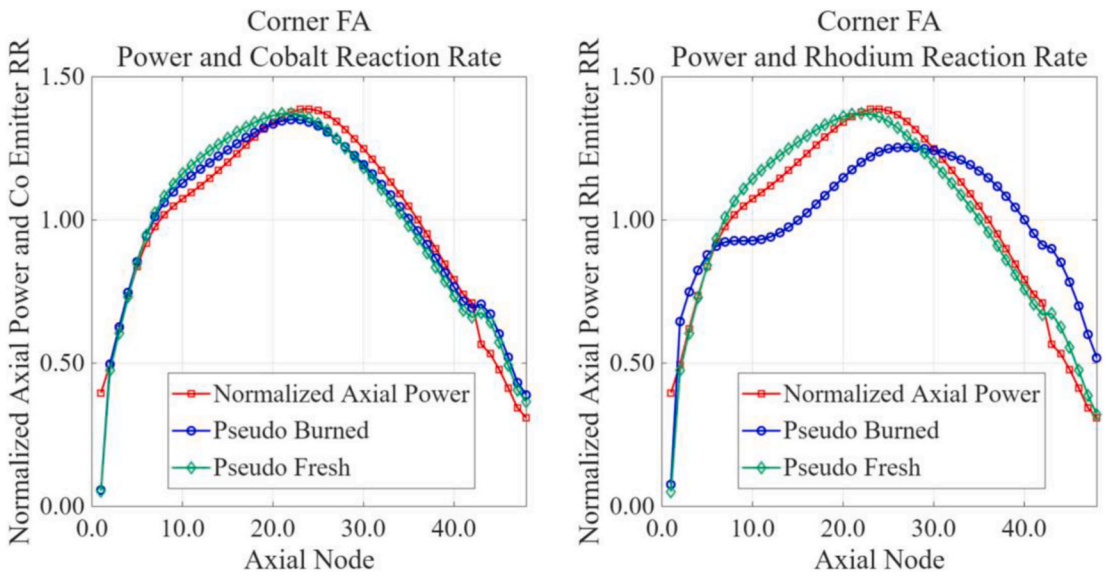


**Fig. 19.** Power of assembly and reaction rate of cobalt and rhodium emitter, using pseudo method, at the EOC, fresh and burned emitter number density are used.

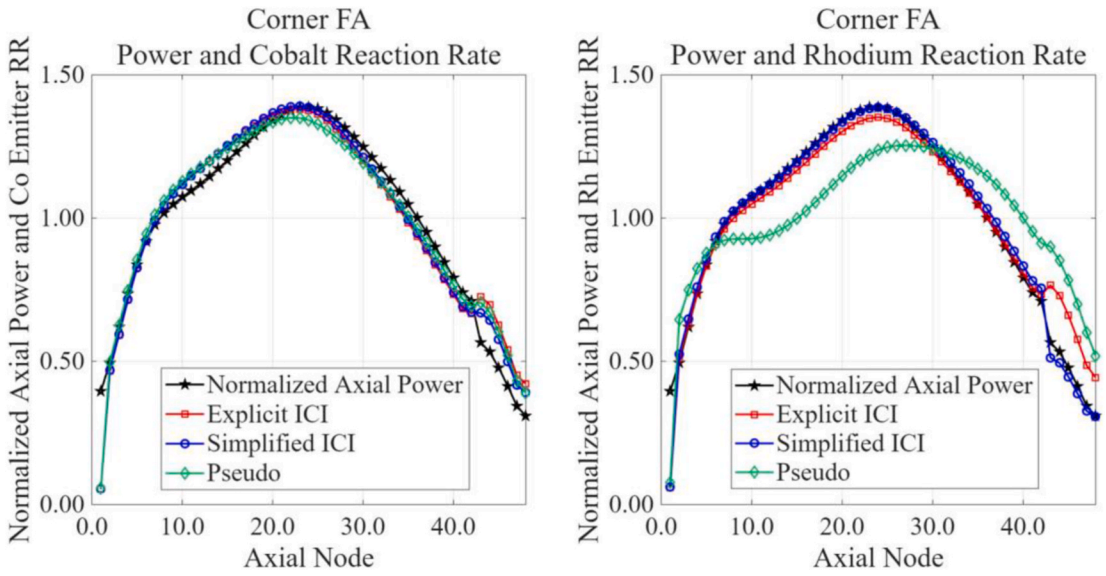


**Fig. 20.** Power of assembly and reaction rate of cobalt and rhodium emitter, at the EOC, burned emitter number density are used in terms of modeling methods.

shift in the critical control rod position, ranging from 2 to 6 cm, compared to the pseudo method results. While the pseudo method exhibited substantial errors (up to 20% relative difference) in correlating SPND reaction rates with assembly power at EOC, both explicit and simplified models accurately captured the burnup-dependent behavior of the emitter nuclides. Furthermore, these models yielded assembly power results consistent with high-fidelity calculations.

In conclusion, the proposed simplified ICI modeling scheme provides an indispensable and balanced approach for reactor core analysis. Its high accuracy, coupled with excellent computational efficiency, is essential for the precise design, operation, and evaluation of Instrumentation and Control (I&C) systems in next-generation reactors. This is particularly critical for advanced concepts like boron-free SMRs that demand highly accurate real-time core information.

## CRediT authorship contribution statement

**Kyeongwon Kim:** Writing – original draft, Visualization, Methodology, Investigation, Formal analysis, Conceptualization. **Dongmin Yun:** Writing – original draft, Methodology, Investigation, Formal analysis, Conceptualization. **Wonkyeong Kim:** Writing – review & editing, Software, Methodology. **Sung Ju Kwon:** Writing – review & editing, Supervision, Project administration, Funding acquisition, Conceptualization. **Setiawan Fathurrahman:** Methodology. **Deokjung Lee:** Writing – review & editing, Supervision, Project administration, Conceptualization.

## Declaration of competing interest

The authors declare that they have no known competing financial interests or personal relationships that could have appeared to influence the work reported in this paper.

## Acknowledgements

This work was supported by the Innovative Small Modular Reactor

Development Agency grant funded by the Korea Goverment (RS-2023-00265742)

## References


[1] C. Kong, D. Lee, H.C. Shin, Lifetime extension of in-core self-powered neutron detector using new emitter materials, Int. J. Energy Res. 41 (2017) 2405–2412, https://doi.org/10.1002/er.3817.

[2] X. Wu, L. Cai, X. Zhang, T. Wu, J. Jiang, Analysis of signal cable noise currents in nuclear reactors under high neutron flux irradiation, Nucl. Eng. Technol. 55 (2023) 4628–4636, https://doi.org/10.1016/j.net.2023.08.044.

[3] F. Khoshahval, M. Park, H.C. Shin, P. Zhang, D. Lee, Vanadium, rhodium, silver and cobalt self-powered neutron detector calculations by RAST-K v2.0, Ann. Nucl. Energy 111 (2018) 644–659, https://doi.org/10.1016/j.anucene.2017.09.048.

[4] J. Park, W. Kim, Y. Kang, W. Jeong, C. Lim, J. Yoon, D. Lee, Development of cross-section model of two-step code system considering control rod depletion for soluble boron free operation of SMR, Prog. Nucl. Energy 189 (2025) 105951, https://doi.org/10.1016/j.pnucene.2025.105951.

[5] B. Koo, D. Hwang, W. In, J. Song, Design features and thermal margin assessment of core protection and monitoring systems of an integral reactor, SMART, J. Nucl. Sci. Technol. 51 (2014) 390–404, https://doi.org/10.1080/00223131.2014.864456.

[6] S. Choi, H. Lee, S.G. Hong, D. Lee, Resonance self-shielding methodology of new neutron transport code STREAM, J. Nucl. Sci. Technol. 52 (2015) 1133–1150, https://doi.org/10.1080/00223131.2014.993738.

[7] J. Choe, S. Choi, P. Zhang, J. Park, W. Kim, H.C. Shin, H.S. Lee, J.E. Jung, D. Lee, Verification and validation of STREAM/RAST-K for PWR analysis, Nucl. Eng. Technol. 51 (2019) 356–368, https://doi.org/10.1016/j.net.2018.10.004.

[8] H. Lee, W. Kim, P. Zhang, M. Lemaire, A. Khassenov, J. Yu, Y. Jo, J. Park, D. Lee, MCS – a Monte Carlo particle transport code for large-scale power reactor analysis, Ann. Nucl. Energy 139 (2020) 107276, https://doi.org/10.1016/j.anucene.2019.107276.

[9] G.M. Lee, J.W. Kim, K.H. Jeoung, T.W. Kim, K.B. Park, K.K. Kim, A Mechanical Characteristic of the In-core Instrument Assembly for Pressurized Water Reactor, KAERI, 2008, pp. 1–24. KAERI/TR-3613/2008.

[10] S. Choi, A. Khassenov, D. Lee, Resonance self-shielding method using resonance interference factor library for practical lattice physics computations of LWRs, J. Nucl. Sci. Technol. 53 (2016) 1142–1154, https://doi.org/10.1080/00223131.2015.1095686.

[11] R.J.J. Stamm'ler, M.J. Abbate, Methods of Steady-State Reactor Physics in Nuclear Design, Academic Press, London, 1983.